Platinum germanides for mid- and long-wave infrared plasmonics

Justin W. Cleary,[1*] William H. Streyer,[2] Nima Nader,[1,3] Shiva Vangala,[1,3] Ivan Avrutsky,[4] Bruce Claflin, [1] Joshua Hendrickson, [1] Daniel Wasserman,[2] Robert E. Peale,[5] Walter Buchwald,[6] and Richard Soref[6]

[1]*Air Force Research Laboratory, Sensors Directorate, Wright-Patterson Air Force Base, Ohio, 45433, USA*
[2]*Department of Electrical and Computer Engineering, University of Illinois, Urbana-Champaign, IL 61801, USA*
[3]*Solid State Scientific Corporation, Nashua, NH 03060, USA*
[4]*Department of Electrical and Computer Engineering, Wayne State University, Detroit, MI 48202, USA*
[5]*Department of Physics, University of Central Florida, Orlando FL, 32816, USA*
[6]*The Engineering Program, University of Massachusetts at Boston, Boston, MA 02125, USA*
**Justin.Cleary.1@us.af.mil*

Abstract: Platinum germanides (PtGe) were investigated for infrared plasmonic applications. Layers of Pt and Ge were deposited and annealed. X-ray diffraction identified $PtGe_2$ and Pt_2Ge_3 phases, and x-ray photo-electron spectroscopy determined vertical atomic composition profiles for the films. Complex permittivity spectra were measured by ellipsometry over the 2 to 15 μm wavelength range. Surface plasmon polariton (SPP) characteristics such as propagation length and field penetration depth were calculated. Photon-to-SPP couplers in the form of 1D lamellar gratings were fabricated and characterized in the range 9 - 10.5 μm via wavelength-dependent specular reflection spectra for multiple angles of incidence. The observed resonances compare well with calculated spectra for SPP excitation on $PtGe_2$. Platinum germanides are CMOS compatible and may serve as SPP hosts for on-chip mid-IR plasmonic components with tighter field confinement than noble-metal hosts.

OCIS codes: (240.6680) Surface plasmons; (130.3060) Infrared; (130.5990) Semiconductors; (160.4670) Optical materials; (230.7370) Waveguides; (280.4788) Optical sensing and sensors.

References and links

1. R. Soref, J. Hendrickson, and J. W. Cleary, "Mid- to long-wavelength infrared plasmonic-photonics using heavily doped n-Ge/Ge and n-GeSn/GeSn heterostructures," Opt. Express **20**(4), 3814–3824 (2012).
2. R. Soref, R. E. Peale, and W. Buchwald, "Longwave plasmonics on doped silicon and silicides," Opt. Express **16**(9), 6507–6514 (2008).
3. J. W. Cleary, G. Medhi, R. E. Peale, W. Buchwald, O. Edwards, and I. Oladeji, "Infrared surface plasmon resonance biosensor," Proc. SPIE **7673**, 767306 (2010).
4. J. W. Cleary, R. E. Peale, D. Shelton, G. D. Boreman, R. Soref, and W. Buchwald, "Silicides for infrared surface plasmon resonance biosensors," Proc. MRS 1133–AA10–03 (2008).
5. M. Shahzad, G. Medhi, R. E. Peale, W. R. Buchwald, J. W. Cleary, R. Soref, G. D. Boreman, and O. Edwards, "Infrared surface plasmons on heavily doped silicon," J. Appl. Phys. **110**(12), 123105 (2011).
6. J. C. Ginn, R. L. Jarecki, Jr., E. A. Shaner, and P. S. Davids, "Infrared plasmons on heavily-doped silicon," J. Appl. Phys. **110**(4), 043110 (2011).
7. S. Law, D. C. Adams, A. M. Taylor, and D. Wasserman, "Mid-infrared designer metals," Opt. Express **20**(11), 12155–12165 (2012).
8. J. W. Cleary, M. R. Snure, K. D. Leedy, D. C. Look, K. Eyink, and A. Tiwari, "Mid- to long-wavelength infrared surface plasmon properties in doped zinc oxides," Proc. SPIE **8545**, 854504 (2012).
9. G. V. Naik, J. Kim, and A. Boltasseva, "Oxides and nitrides as alternative plasmonic materials in the optical range," Opt. Mater. Express **1**(6), 1090–1099 (2011).
10. S. Law, V. Podolskiy, and D. Wasserman, "Towards nano-scale photonics with micro-scale photonics; the opportunities and challenges of mid-infrared plasmonics," J. Nanophotonics A **24**, 103–130 (2013).
11. G. V. Naik, V. M. Shalaev, and A. Boltasseva, "Alternative plasmonic materials: beyond gold and silver," Adv. Mater. **25**(24), 3264–3294 (2013).

#224217 - $15.00 USD Received 2 Oct 2014; revised 10 Dec 2014; accepted 16 Jan 2015; published 4 Feb 2015

12. J. W. Cleary, R. E. Peale, D. J. Shelton, G. D. Boreman, C. W. Smith, M. Ishigami, R. Soref, A. Drehman, and W. R. Buchwald, "IR permittivities for silicides and doped silicon," J. Opt. Soc. Am. B **27**(4), 730–734 (2010).
13. S. Gaudet, C. Detavernier, A. J. Kellock, P. Desjardins, and C. Lavoie, "Thin film reaction of transition metals with germanium," J. Vac. Sci. Technol. **24**(3), 474–485 (2006).
14. E. D. Palik, *Handbook of Optical Constants of Solids* (Academic, 1988).
15. H. Raether, *Surface Plasmons on Smooth and Rough Surfaces and on Gratings* (Springer, 1988).
16. I. Avrutsky, R. Soref, and W. Buchwald, "Sub-wavelength plasmonic modes in a conductor-gap-dielectric system with a nanoscale gap," Opt. Express **18**(1), 348–363 (2010).
17. D. M. Whittaker and I. S. Culshaw, "Scattering-matrix treatment of patterned multilayer photonic structures," Phys. Rev. B **60**(4), 2610–2618 (1999).
18. M. Liscidini, D. Gerace, L. C. Andreani, and J. E. Sipe, "Scattering-matrix analysis of periodically patterned multilayers with asymmetric unit cells and birefringent media," Phys. Rev. B **77**(3), 035324 (2008).
19. H. Okamoto, "The Ge-Pt system (germanium-platinum)," J. Phase Equilibria **13**(4), 413–417 (1992).
20. J. W. Cleary, G. Medhi, R. E. Peale, and W. R. Buchwald, "Long-wave infrared surface plasmon grating coupler," Appl. Opt. **49**(16), 3102–3110 (2010).

1. Introduction

Plasmonic devices confine and guide electromagnetic waves at sub-wavelength dimensions. Applications include chip-scale integrated "plasmonic-photonics" and optoelectronic circuits [1, 2] and novel approaches to sensing [3, 4]. Noble metals have been the default surface plasmon polariton (SPP) hosts at visible wavelengths, since their plasma frequencies are in the short-wavelength visible or near UV, the real parts of their permittivity are strongly negative in the visible, and the imaginary parts are relatively small. Noble metals, however, fail to confine SPPs to useful scales in the mid-infrared. Sub-wavelength mode confinement requires that the plasma frequency be closer to the operational frequencies. Doped semiconductors, such as Si, Ge, and related alloys [1, 5, 6], InAs [7], and metal oxides [8, 9] have been investigated as design-tunable plasmonic materials for the infrared. The carrier concentrations achievable by doping in practical semiconductors are less than $\sim 10^{21}$ cm^{-3}, which may not be efficiently repeatable in all of the aforementioned materials. This limits the shortest plasma wavelengths to wavelengths beyond ~2 μm which in turn may limit plasmonic propagation lengths in the mid-infrared. Comprehensive reviews of infrared plasmonic materials can be found in [10, 11].

We report here the investigation of germanides as new SPP host materials with plasma wavelengths in the near-infrared and at shorter wavelengths that doped semiconductors can offer. These may help bridge the gap between the doped semiconductors and metals. These SPP hosts are more compatible with conventional semiconductor device processing than are metal oxides. These new materials will enable sensors based on infrared SPPs that have adequate confinement and propagation length. Specifically envisioned are plasmonic-photonic hybrid waveguides [1] that operate in the mid-IR.

Metal silicides [12] have been shown to have NIR plasma frequencies. Metal germanides are expected to be similar. Germanium is an excellent dielectric for the migration of plasmonic-photonics wavelengths beyond 2 μm, where it is transparent. Germanium hybrid plasmonic-photonic waveguides are an excellent candidate for creating a new on-chip technology because intrinsic Ge has higher infrared transparency over the 8 to 15 μm band than does silicon which suffers from phonon absorption in that range. Metal germanides are obvious candidates for the construction of new Ge-based hybrid waveguides. Among those germanides, platinum germanides may be a leading candidate due to the multiple phases possible [13] and formation at low anneal temperatures. Platinum germanide is the subject of this paper, though other metals like Pd, Ni, and Cu, can be used readily to create germanides with expected performance similar to that of PtGe in the same way that Pd-, Ni-, and Cu-silicides demonstrate similar optical properties to PtSi [12].

2. Platinum Germanide Films

Films were formed on p-type Si wafers with vendor-specified 0.001-0.005 ohm-cm resistivity. The wafer substrates were cleaned in O_2 plasma, and then 200 nm of germanium

#224217 - $15.00 USD Received 2 Oct 2014; revised 10 Dec 2014; accepted 16 Jan 2015; published 4 Feb 2015

followed by 50 nm of platinum were electron-beam evaporated onto them. The wafers were then cut into 1 cm x 1 cm squares. The total film thickness of 250 nm was confirmed by scanning electron microscope (SEM) cross sectional imaging. Anneals in a nitrogen purged tube furnace were completed in the range 300-500°C for 45 minutes as described in Table 1. Two samples were annealed simultaneously separated longitudinally in the tube by a few millimeters, so that temperature differences were slight.

Table 1. PtGe films with evaporated structure of 50 nm Pt / 200 nm Ge / Si substrate. Anneal times were 45 minutes.

Sample	Anneal Temperature (°C)
Unannealed	-
A1, A2	300
B1, B2	350
C1, C2	400
D1, D2	450
E1, E2	500

IR ellipsometry (J. A. Woollam IR-VASE) was used to determine the complex optical constants for the films. First, an uncoated Si substrate and a substrate with 200 nm of electron beam evaporated Ge were measured. The Woollam WVASE32 software was used to determine the complex permittivity. The unannealed Pt/Ge structure was then measured and analyzed, to determine the Pt permittivity. Finally, the annealed films were similarly characterized taking into account the 250 nm film thickness and the Si substrate permittivity.

Figure 1 presents the measured Pt and PtGe complex permittivity spectra ε. The former confirm the published Pt values [14] (not shown) except that Im(ε) for our Pt film is ~twice larger in the IR. Samples A-D all have similar spectra. Their average, excluding B2, is plotted in Fig. 1 as the dark blue line with the standard deviation being represented by the light blue band. Sample B2 was discolored and its permittivity was very different, suggesting contamination. The magnitude of the real part is somewhat larger than the imaginary part at 2.5 μm, but at 15 μm, this situation is reversed.

The permittivity of samples E-1 and E-2 (red-line with light-red uncertainty band) were much less metallic than the A-D samples, which were annealed at lower temperatures. The imaginary part of ε for both E samples is nearly 10x smaller than the real part at 15 μm wavelength. Empirical values for PtSi are also plotted for comparison [12]. These spectra contain the Si-O absorption at 8 μm. The absence of this feature for all of the PtGe samples confirms the unimportance of Si substrate contributions to the germanide permittivity spectra in Fig. 1.

#224217 - $15.00 USD Received 2 Oct 2014; revised 10 Dec 2014; accepted 16 Jan 2015; published 4 Feb 2015

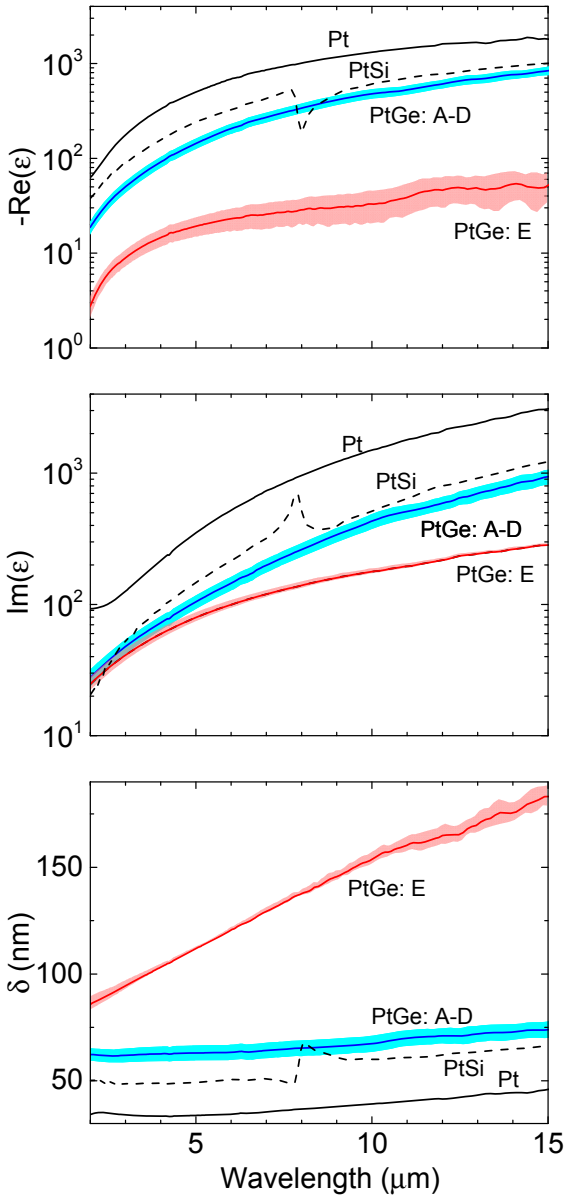

Fig. 1. Measured real (top) and imaginary (middle) parts of the permittivity for Pt and PtGe, and calculated optical skin depth (bottom). Solid lines indicate average values while shaded bands represent standard deviation. Results for PtSi [12] and for Pt are presented for comparison.

The optical skin depth, i.e. the characteristic 1/e penetration depth for field determined from Beers law is

$$\delta = \left[\frac{2\pi}{\lambda} \mathrm{Im}\sqrt{\varepsilon} \right]^{-1}, \qquad (1)$$

where λ is the free space wavelength. The δ spectrum calculated from the measured permittivity is presented in Fig. 1 (bottom). The skin depths for A-D and PtSi samples are much less than the film thicknesses, which were 250 and 200 nm, respectively. Only for E

#224217 - $15.00 USD Received 2 Oct 2014; revised 10 Dec 2014; accepted 16 Jan 2015; published 4 Feb 2015

samples, and only beyond 10 μm wavelength, does the skin depth approach the film thickness, such that contributions from the substrate become significant. This is roughly the same wavelength range where fringes begin appearing in the real part of ε for the E samples. Nevertheless, these effects are small compared with the generally Drude-like spectrum of the platinum germanide.

Figure 2 presents X-ray diffraction (XRD) measurements taken in asymmetric out-of-plane configuration with the incident angle at the substrate of 15° and using the $CuK\alpha_1$ line at 1.5406 Å wavelength. The observed peaks arise from the polycrystalline films, and no peaks were observed from the Si substrate. The unannealed sample confirms the presence of polycrystalline platinum. A shallow and broad peak in the unannealed sample is due to as-deposited amorphous Ge and was treated as background and subtracted. Sample C1 represents samples annealed at low temperature, which have similar permittivity. Comparing the observed peaks with International Center for Diffraction Data (ICDD) identifies the A-D films as mainly $PtGe_2$. Sample E1 appears to be Pt_2Ge_3 with a small amount of PtGe indicated by red square symbols, while for sample E2 the contribution of PtGe (peaks indicated by red "X"s) is much weaker. The E samples will be referred to as Pt_2Ge_3.

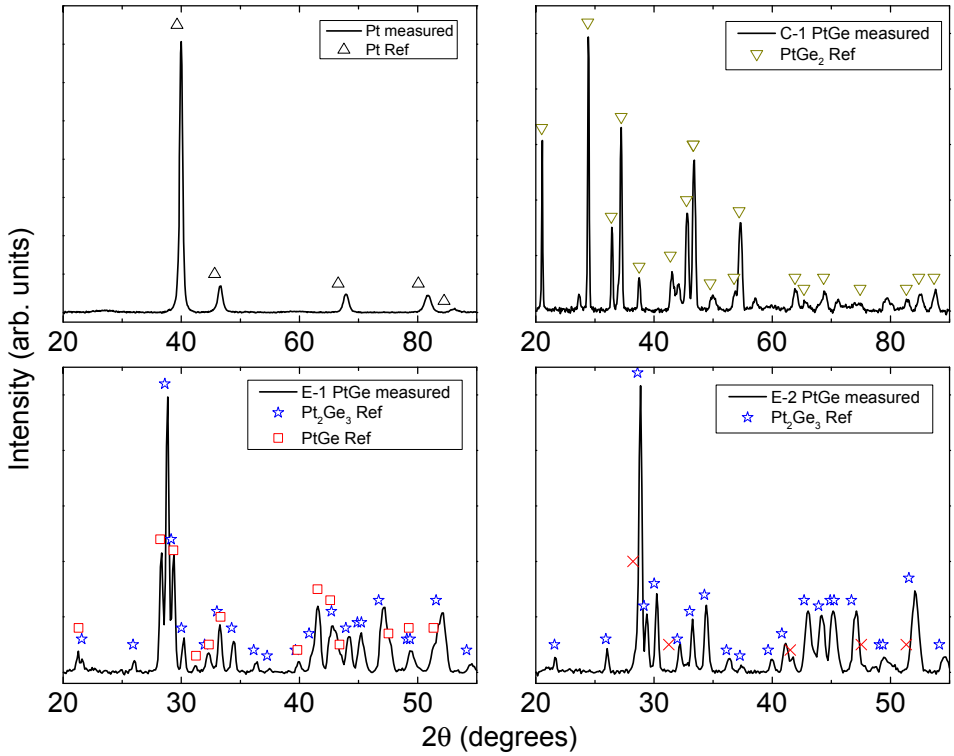

Fig. 2. XRD spectra of unannealed Pt (upper-left), and annealed samples C-1 (upper-right), E-1 (lower-left), and E-2 (lower-right).

The XRD data for the annealed samples cannot exclude the possible presence of platinum silicides, e.g. Pt_2Si_3 and PtSi, since some of the silicide peaks coincide with those of platinum-germanide in the database. However, none of the peaks observed in Fig. 2 belongs exclusively to a silicide. The very long anneal times do potentially allow interdiffusion of Pt and Si, although this only occurs near the substrate as will be shown shortly. Thus, the bulk of the films are predominantly the indicated platinum germanide.

#224217 - $15.00 USD Received 2 Oct 2014; revised 10 Dec 2014; accepted 16 Jan 2015; published 4 Feb 2015

The films also were characterized via scanning electron microscopy (SEM). SEM images are presented in Fig. 3 for samples C1 and E2. For C1, where the XRD data indicated the material is $PtGe_2$, the film is fairly uniform with grain sizes on the order of hundreds of nm. The SEM images of E1 and E2, which were similar to each other, revealed a mosaic of dark and light features, both at the surface and in the film as seen in Fig. 3 (bottom), with 1 micron length scale, suggesting a segregated mixture of two materials in agreement with XRD results.

Figure 4 presents X-ray photoelectron spectra (XPS), which were recorded after iterative sputtering steps to determine the vertical distributions of Ge, Pt and Si. The unannealed sample of 50 nm Pt on 200 nm Ge confirmed the as-deposited materials and determined the uncertainty in the position of the interfaces to be ~10 minutes of sputtering time. For Pt, a 50 nm thickness corresponds to 10 min of sputtering time, but the Ge layer's 200 nm thickness requires ~30 min sputtering time, i.e. Ge sputters ~1.3x faster. The Si substrate first appears at a sputtering time of 40 min.

After annealing, the Pt and Ge appear uniformly mixed. Since the difference in sputtering rates for Pt and Ge is fairly small, we may assume that the integrated time for Pt followed Ge is the about same as for germanide. Then the XPS results show germanide thicknesses with uniform composition of nearly 200 nm in both annealed samples. After annealing, the interface with the Si substrate appears 10 minutes earlier due to upward diffusion of silicon. This intermixing region is not more than ~50 nm thick. The data do not suggest that Ge diffuses into Si, because if anything, the Ge tail gets shorter. Pt diffused freely through the Ge and partly into the Si. From the tails, the interdiffusion of E samples is more than for the C sample. The XPS data indicates that any silicide within 50 nm of the original substrate boundary, confirming that silicide would not be probed by the ellipsometry measurements.

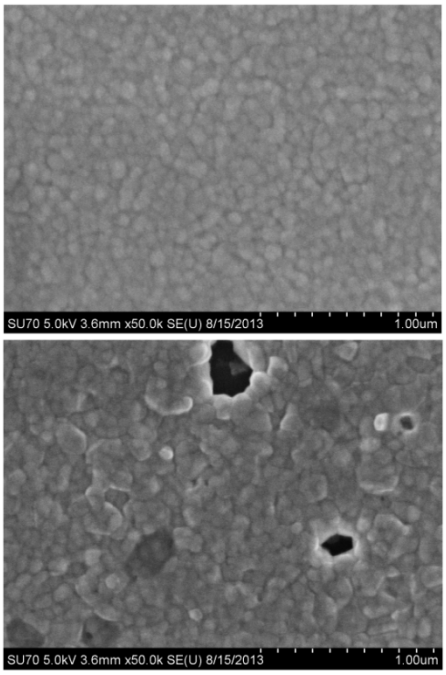

Fig. 3. SEM images of PtGe films annealed at 400°C (C1, top) and 500°C (E2, bottom).

#224217 - $15.00 USD Received 2 Oct 2014; revised 10 Dec 2014; accepted 16 Jan 2015; published 4 Feb 2015

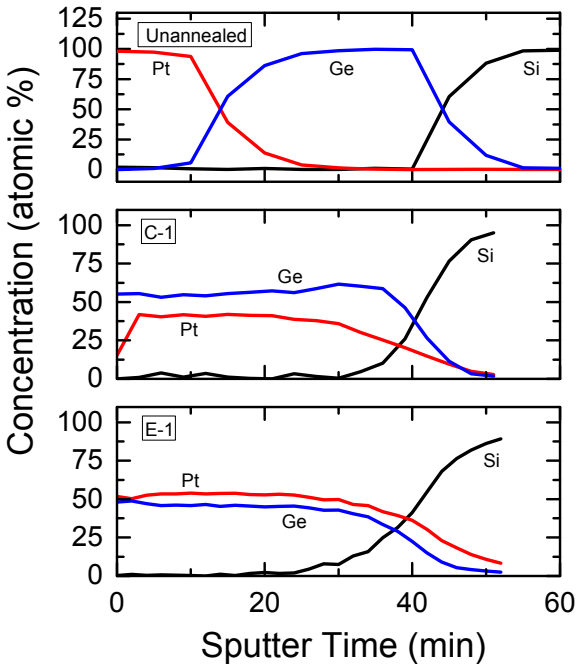

Fig. 4. XPS data for unannealed Pt, and annealed samples C-1and E-2 as a function of sputter time.

3. Surface Plasmon Polariton Properties

The utility of a particular SPP host material for plasmonic applications at a given wavelength is based on metrics, including the SPP field confinement and propagation length. The 1/e SPP field penetration depth from the interface into the dielectric (d) or conductor (c), which is a measure of mode confinement, is [15]

$$L_{d,c} = \left[\frac{2\pi}{\lambda} \mathrm{Re} \sqrt{\frac{-\varepsilon_{d,c}^{\ 2}}{\varepsilon_d + \varepsilon_c}} \right]^{-1} . \tag{2}$$

The plasmon intensity propagation length is [15]

$$L_x = \left[2 \,\mathrm{Im}\, k_{SPP} \right]^{-1} , \tag{3}$$

where the SPP wavevector is

$$k_{SPP} = \frac{2\pi}{\lambda} \sqrt{\frac{\varepsilon_d \, \varepsilon_c}{\varepsilon_d + \varepsilon_c}} . \tag{4}$$

Figure 5 presents calculated spectra for these parameters over the wavelength range 2 to 15 μm when the dielectric is air with permittivity of unity. With increasing wavelength the real part of the conductor's permittivity becomes more negative, while the propagation length and penetration depth increase. Figure 5 indicates that $PtGe_2$ provides about twice tighter mode confinement throughout the IR compared with Pt, while the propagation length on $PtGe_2$ is 2.5 to 4 times smaller. $PtGe_2$ achieves a slight improvement in terms of field confinement over PtSi, though the propagation length is correspondingly smaller. Pt_2Ge_3 provides the

#224217 - $15.00 USD Received 2 Oct 2014; revised 10 Dec 2014; accepted 16 Jan 2015; published 4 Feb 2015

tightest confinement and the shortest propagation length of any of the studied materials with these being 2 to 3 and 10 to 14 times smaller, respectively, than platinum.

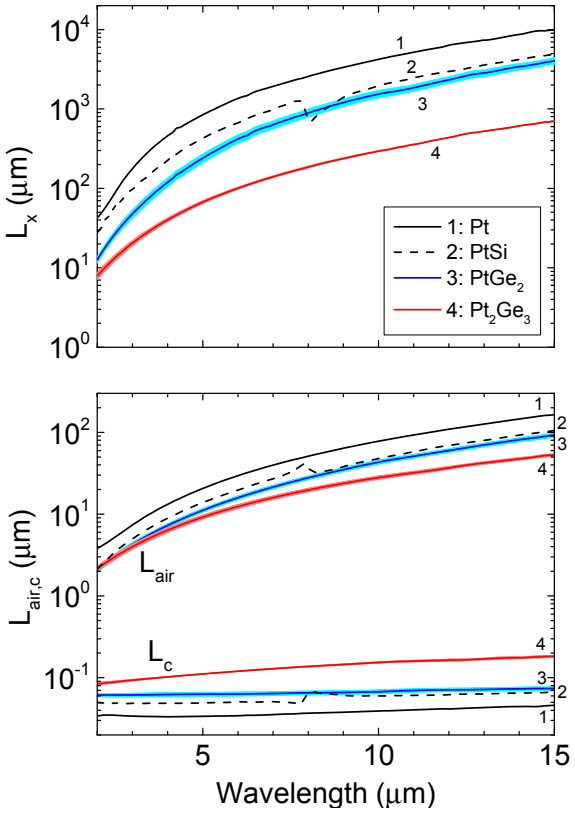

Fig. 5. Plasmon energy propagation lengths (top) and field penetration depths (bottom) for Pt, PtSi, $PtGe_2$, and Pt_2Ge_3. The solid lines are calculated from measured permittivity spectra. Shading indicates the uncertainty. The dashed lines show PtSi results from data in [12].

Now we investigate practical limits for waveguide applications in integrated photonic and plasmonic circuits using the same criteria as in [2]. We suppose that the SPP host material is useful when the field penetration depth into the dielectric L_{air} is less than three times the wavelength; e.g. for $PtGe_2$, we see from Fig. 5 (bottom) that this holds for wavelengths smaller than about 6.9 μm. This criteria also establishes a long wavelength limit for SPP applications of λ_{max} = 11.7 μm for Pt_2Ge_3. Table 2 presents λ_{max} values for the studied materials together with SPP properties at those wavelengths. For comparison to a representative noble metal, λ_{max} for gold is 3 μm [2], effectively removing this standard material from consideration as an SPP host for MIR applications. Pt has only a slightly longer cutoff wavelength than gold: λ_{max} = 3.7 μm. PtSi, $PtGe_2$, and Pt_2Ge_3 are successively more interesting for the MIR. Pt_2Ge_3 provides the tightest confinement at all wavelengths, but L_x for Pt_2Ge_3 is smaller than for $PtGe_2$ by a factor of 3-6. A minimum useful wavelength where L_x exceeds two wavelengths has also been established [2]. This value is at least tens of microns for all materials, so that this criteria is satisfied for all of the measured range.

The longer propagation length for $PtGe_2$ over Pt_2Ge_3 is explained by its 2-3 times smaller penetration depth into the conductor at λ_{max}. At a wavelength of 5 μm the penetration depths into the conductor of $PtGe_2$ and Pt_2Ge_3 are 0.063 and 0.11 μm, respectively. For this specific wavelength, the thickness of $PtGe_2$ plasmonic waveguides will be ~60% of an equivalent Pt_2Ge_3 waveguide (as determined by penetration depth into the conductor), requiring

#224217 - $15.00 USD Received 2 Oct 2014; revised 10 Dec 2014; accepted 16 Jan 2015; published 4 Feb 2015

thicknesses of ~100 nm or less, well suited for on-chip nanophotonic applications. For these reasons $PtGe_2$ may be a more useful overall plasmonic waveguide host than Pt_2Ge_3.

Table 2. Predicted practical performance of plasmonic waveguides. L_x, L_{air}, and L_c are the corresponding values at the upper wavelength limit.

Material	Practical Upper Limit λ_{max} (μm)	L_x (μm)	L_{air} (μm)	L_c (μm)
Pt	3.7	347	11	0.033
PtSi	5.4	532	16	0.050
$PtGe_2$	6.9	615	21	0.064
Pt_2Ge_3	11.7	410	35	0.163

The foregoing calculations assumed plasmonic waveguides formed at the interface between a conductor and air. Longer propagation lengths may also be achieved using more confining materials such as Pt_2Ge_3 by using so-called "gap-plasmon" waveguides [16]. These may be formed using platinum germanide by first depositing a low index thin-film "gap dielectric" on a germanium strip, followed by sequential deposition of Ge and Pt, and then annealing to create the platinum germanide covered gap. Many other possible architectures exist.

4. 1D Pt and PtGe Surface Plasmon Grating Couplers

Pt and PtGe 1D lamellar grating couplers were fabricated with 20 μm period and nominal 50% duty cycle. Silicon wafers were photolithographically patterned by deep reactive ion etching to ~1 μm depth, followed by Pt and Ge deposition and annealing. Figure 6 (top) presents the measured profile with the actual duty cycle being near ~50% while confirming the 1 μm depth. The profile shows the tops of the gratings bars as being ~1.5x the bottoms with the gratings having well rounded edges which are both likely artifacts due to the finite tip width and non-uniform scan rate. An SEM image (Fig. 6 bottom) of a $PtGe_2$ grating annealed at 350°C shows good surface quality. XRD on the same grating confirms the expected $PtGe_2$ composition.

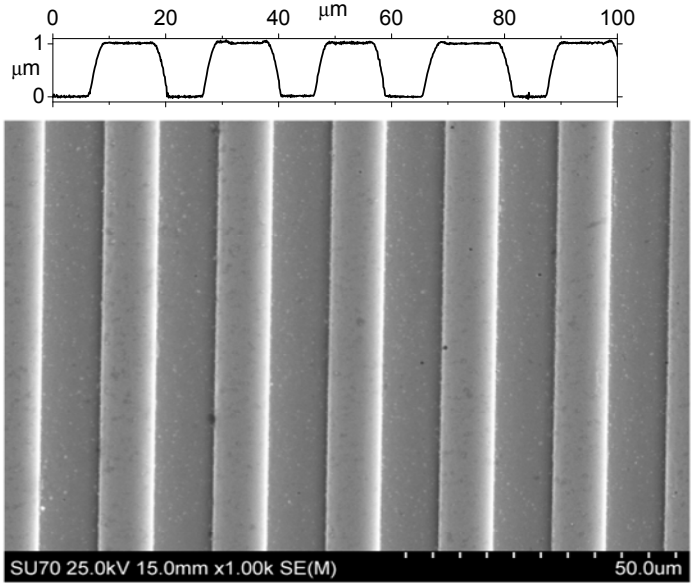

Fig. 6. Profile (top) and SEM image (bottom) of fabricated $PtGe_2$ 1D lamellar grating. The vertical scale of the profile is exaggerated 10x compared to the horizontal scale.

#224217 - $15.00 USD Received 2 Oct 2014; revised 10 Dec 2014; accepted 16 Jan 2015; published 4 Feb 2015

Figure 7 presents a schematic of the experiment for measuring SPP excitation resonances. Gratings were mounted and aligned on a manual rotation stage with markings every 2 degrees. Angular uncertainty was estimated to be 0.5 deg. Specularly-reflected TM-polarized quantum cascade laser (Daylights Solutions) light was collected by a 77 K HgCdTe detector for different fixed angles of incidence while sweeping the wavelength. A spectrum at 45° incidence, where no SPP feature occurs, was used to normalize the data. The SPP coupling condition is

$$\mathrm{Re}\left[k_{SPP}\right]*sign(m)=\frac{2\pi}{\lambda}\left[\sin\left(\theta\right)+\frac{m\lambda}{P}\right]. \qquad (5)$$

In Eq. (5), θ is angle of incidence, m is the SPP mode order (positive or negative integer), and P is the grating period.

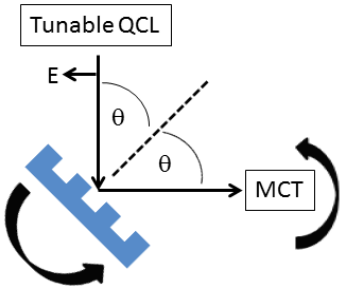

Fig. 7. Angular-dependent reflection experimental setup used for characterizing gratings.

Figure 8 (left) presents the specular reflection spectra for an unannealed Pt grating and the $PtGe_2$ grating for multiple incidence angles. Plotted in Fig. 8 (right) are calculated reflection spectra for the angles matching the experimental configurations with the same nominal sample layer structure, e.g. 250 nm of either $PtGe_2$ or Pt/Ge films on the top and in the valley of the silicon grating. The calculations use the scattering matrix algorithm which is described in [17, 18]. The excitation conditions corresponding to the 1 and −3 SPP mode orders are determined according to Eqs. (4-5) and are plotted as symbols. Only one symbol is shown for each resonance since the excitation wavelengths are within ~0.1% for the three materials. The negative order indicates that the SPP propagates in the direction opposite to the projection of the incident wavevector on the plane. Clear dips in reflection occur when SPPs are excited. The reflection spectra for $PtGe_2$ are as sharp as those for the unannealed Pt on Ge sample. The slight spectral shift between them can be attributed to uncertainty in angular positioning. Due to a 0.5 degree experimental angular uncertainty, it was necessary to consider the incidence angle as a fitting parameter to achieve the best agreement. For the nominal 30 and 32.5 degree experimental angles, calculations at 30.5 and 33° agree best, respectively (shown in Fig. 8 right). The resonance wavelengths calculated from Eq. (5) agree well with the low-wavelength edge of the calculated resonances. Calculations and measurements for $PtGe_2$ gratings formed from annealing at temperatures other than 350°C agree closely with the spectra shown in Fig. 8. The similarity in $PtGe_2$ and Pt-on-Ge resonances indicates comparable photon-to-SPP coupling efficiency, with the former having the advantage of twice better confinement at these wavelengths as discussed earlier. Slight discrepancies between experimental and calculated lineshapes could be due to thin sidewall coatings that are apparent in actual gratings but not accounted for in the calculations.

Gratings annealed at 500°C for characterizing Pt_2Ge_3 SPP resonances were determined by XRD to be $PtGe_2$, so that the appearance of Pt_2Ge_3 in the unstructured films is an outlier of unknown cause. It is conceivable that the films used for the initial 500°C anneals had slightly thicker Pt, increasing its atomic percentage, which may result in Pt_2Ge_3 according to [19] although there are a number of other parameters during fabrication such as temperature,

#224217 - $15.00 USD Received 2 Oct 2014; revised 10 Dec 2014; accepted 16 Jan 2015; published 4 Feb 2015

anneal time or quenching that may have allowed the formation of this composition. Attempts to reproduce the formation of Pt_2Ge_3 were unsuccessful. Thus there are no experimental resonances to compare with the calculated Pt_2Ge_3 spectra (red dotted lines in Fig. 8 right) due to the noted complexities in formation of platinum germanides. Their calculated resonances are significantly broadened relative to the Pt-on-Ge and $PtGe_2$ resonances. However, coupling of light into SPPs on Pt_2Ge_3 should still be effective. Coupling may be optimized by investigating grating heights [20] and duty cycle. The data presented in Fig. 8 is the first experimental demonstration of SPP generation on platinum germanides to our knowledge.

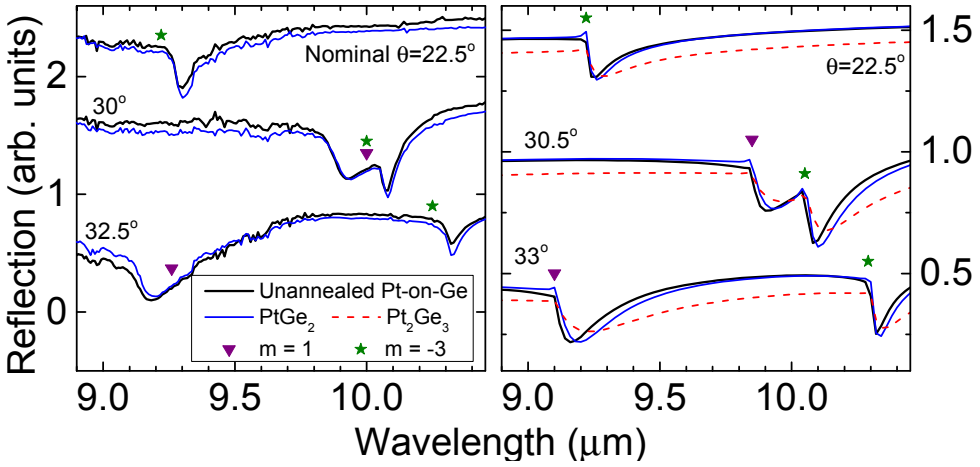

Fig. 8. Wavelength-dependent reflection spectra of Pt and $PtGe_2$. (left) Experimental results using nominal angles and (right) calculations using angles fitted to experiments and based on measured permittivities for unannealed Pt-on-Ge, $PtGe_2$, and Pt_2Ge_3. In these respective calculated cases, the structure was 50 nm Pt on 200 nm Ge or 250 nm platinum germanide on etched Si. Symbols indicate analytically calculated SPP resonance wavelengths for bulk Pt.

5. Summary

Pt and PtGe films, and 1D lamellar gratings coated with them, have been fabricated and investigated at MIR and LWIR wavelengths with emphasis on SPP applications. $PtGe_2$ and Pt_2Ge_3 phases were identified in individual samples and IR optical constants separately determined for them. SPP properties such as propagation length and field penetration depth were calculated from the optical data with favorable predictions regarding MIR and LWIR plasmonic device applications. In particular, platinum germanide SPP hosts offer less loss than heavily doped semiconductors and tighter mode confinement than noble metals. Photon-to-SPP excitation resonances were studied using the gratings, revealing comparable coupling strength for Pt and $PtGe_2$ and agree well with calculations. The materials investigated are CMOS compatible and easy to fabricate. These points suggest platinum germanide as an attractive SPP host for MIR and LWIR plasmonic or "plasmonic-photonic" on-chip components.

Acknowledgments

JWC, NN and WS acknowledge support from AFOSR (Air Force Office of Scientific Research) under LRIR No. 12RY10COR (Program Officer Dr. Gernot Pomrenke). RS appreciates the support of the AFOSR grant FA9550-14-1-0196 and the UK EPSRC project MIGRATION. JRH and IA also acknowledge support from AFOSR (Dr. Pomrenke) under LRIR number 12RY05COR.

#224217 - $15.00 USD Received 2 Oct 2014; revised 10 Dec 2014; accepted 16 Jan 2015; published 4 Feb 2015